

# Computational fluid dynamics

For the flow of an incompressible fluid, if the Navier–Stokes equations of motion and the continuity equation are solved simultaneously under given boundary conditions, an exact solution should be obtained. However, since the Navier–Stokes equations are non-linear, it is difficult to solve them analytically.

Nevertheless, approximate solutions are obtainable, e.g. by omitting the inertia terms for a flow whose  $Re$  is small, such as slow flow around a sphere or the flow of an oil film in a sliding bearing, or alternatively by neglecting the viscosity term for a flow whose  $Re$  is large, such as a fast free-stream flow around a wing. But for intermediate  $Re$ , the equations cannot be simplified because the inertia term is roughly as large as the viscosity term. Consequently there is no other way than to obtain the approximate solution numerically.

For a compressible fluid, it is further necessary to solve the equation of state and the energy equation simultaneously with respect to the thermodynamical properties. Thus, multi-dimensional shock wave problems can only be solved by relying upon numerical solution methods.

Of late, with the progress of computers, it has become popular to solve flow problems numerically. By such means it is now possible to follow a kaleidoscopic change of flow.

This field of engineering is referred to as numerical fluid mechanics or computational fluid dynamics. It can be roughly classified into four approaches: the finite difference method, the finite volume method, the finite element method and the boundary element method.

## 15.1 Finite difference method

### 15.1.1 Finite difference indication

---

One of the methods used to discretise the equations of flow for computational solution is the finite difference method.

The fundamental method for indicating a partial differential coefficient in

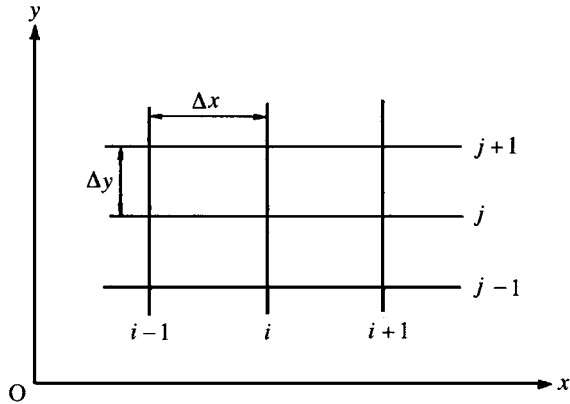


Fig. 15.1 Finite difference method

finite difference form is through the Taylor series expansion of functions of several independent variables. Assume a rectangular mesh, for example. Subscripts  $(i, j)$  are to indicate  $(x, y)$  respectively as shown in Fig. 15.1. The mesh intervals in the  $i$  and  $j$  directions are  $\Delta x$  and  $\Delta y$  respectively, while  $f$  is a functional symbol. Space points  $(i, j)$  mean  $(x_i = x_0 + i\Delta x, y_i = y_0 + j\Delta y)$ .

The forward, backward and central differences of the first-order differential coefficient  $\partial f/\partial x$  can be induced in the manner stated below. Provided that function  $f$  is continuous, permitting Taylor expansion of  $f_{i+1}$  and  $f_{i-1}$ , then considering the  $x$  direction alone,

$$f_{i+1} = f_i + \frac{\partial f}{\partial x} \Big|_i \Delta x + \frac{1}{2} \frac{\partial^2 f}{\partial x^2} \Big|_i \Delta x^2 + \frac{1}{6} \frac{\partial^3 f}{\partial x^3} \Big|_i \Delta x^3 + \dots \quad (15.1)$$

$$f_{i-1} = f_i - \frac{\partial f}{\partial x} \Big|_i \Delta x + \frac{1}{2} \frac{\partial^2 f}{\partial x^2} \Big|_i \Delta x^2 - \frac{1}{6} \frac{\partial^3 f}{\partial x^3} \Big|_i \Delta x^3 + \dots \quad (15.2)$$

Solving eqn (15.1) for  $\partial f/\partial x|_i$ ,

$$\frac{\partial f}{\partial x} \Big|_i = \frac{f_{i+1} - f_i}{\Delta x} + O(\Delta x) \quad (15.3)$$

Here,  $O(\Delta x)$  means the combination of terms of order  $\Delta x$  or less. Since this finite difference approximation, omitting  $O(\Delta x)$ , is approximated by the functional value  $f_i$  of  $x_i$  and functional value  $f_{i+1}$  at  $x_{i+1}$  on the side of increasing  $x$ , it is called the forward difference. This finite difference indication has a truncation error of the order  $\Delta x$  and it is said to have first-order accuracy. The backward difference is approximated by the functional value  $f_{i-1}$  on the side of decreasing  $x$  and  $f_i$  through a similar process, and

$$\frac{\partial f}{\partial x} \Big|_i = \frac{f_i - f_{i-1}}{\Delta x} + O(\Delta x) \quad (15.4)$$

Furthermore, solving eqns (15.1) and (15.2) for  $\partial f/\partial x|_i$ , then by subtraction,

$$\left. \frac{\partial f}{\partial x} \right|_i = \frac{f_{i+1} - f_{i-1}}{2\Delta x} + O(\Delta x^2) \quad (15.5)$$

Since this finite difference representation is approximated by functional values  $f_{i-1}$  and  $f_{i+1}$  on either side of  $x_i$ , it is called the central difference. As seen from eqn (15.5), the central difference is said to have second-order accuracy. This method of representation is also applicable to the differential coefficient for  $y$ .

Next, the central difference for  $\partial^2 f / \partial x^2|_i$  is obtainable by adding eqn (15.1) to eqn (15.2). In other words, it has second-order accuracy:

$$\left. \frac{\partial^2 f}{\partial x^2} \right|_i = \frac{f_{i+1} - 2f_i + f_{i-1}}{2\Delta x^2} + O(\Delta x^2) \quad (15.6)$$

In this way, a partial differential coefficient is expressed in finite difference form as an algebraic equation. By substituting these coefficients a partial differential equation can be converted to an algebraic equation.

## 15.1.2 Incompressible fluid

### *Method using stream function and vorticity*

To begin with, an explanation is given of the case where the flow pattern is obtained for the two-dimensional steady laminar flow of an incompressible and viscous fluid in a sudden expansion of a pipe as shown in Fig. 15.2. In this case, what governs the flow are the Navier–Stokes equations and the continuity equation.

In the steady case, a vorticity transport equation is derived from the Navier–Stokes equation and is expressed in non-dimensional form. It produces the following equation by putting  $\partial \zeta / \partial t = 0$  in eqn (6.18) and additionally substituting the relationship of eqn (12.12),  $u = \partial \psi / \partial y$ ,  $v = -\partial \psi / \partial x$ :

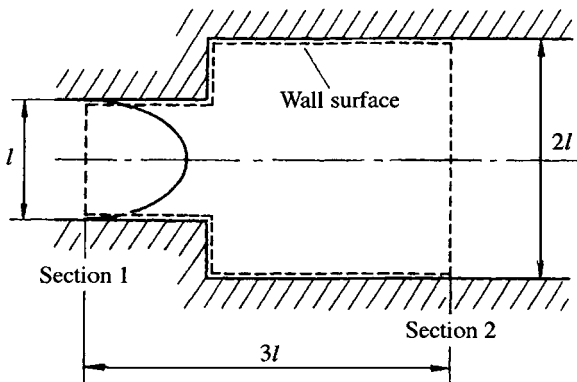


Fig. 15.2 Flow in a sudden expansion

$$\frac{\partial \psi}{\partial y} \frac{\partial \zeta}{\partial x} - \frac{\partial \psi}{\partial x} \frac{\partial \zeta}{\partial y} = \frac{1}{Re} \left( \frac{\partial^2 \zeta}{\partial x^2} + \frac{\partial^2 \zeta}{\partial y^2} \right) \quad (15.7)$$

Also, the vorticity definition equation (4.7) can be expressed in terms of the stream function  $\psi$  using the relationship in eqn (12.12):

$$\frac{\partial^2 \psi}{\partial x^2} + \frac{\partial^2 \psi}{\partial y^2} = -\zeta \quad (15.8)$$

The actual numerical computation is made by approximating the above partial differential equations by finite difference equations. In this computation, since the flow appearing in Fig. 15.2 is symmetric about the centre line, only the lower half of the pipe is the computational area and it is covered by a parallel mesh of interval  $h$  as shown in Fig. 15.3. Using eqns (15.5) and (15.6) for  $\psi$ ,

$$\left. \begin{aligned} \frac{\partial \psi}{\partial x} &\approx \frac{\psi_{i+1,j} - \psi_{i-1,j}}{2h} \\ \frac{\partial \psi}{\partial y} &\approx \frac{\psi_{i,j+1} - \psi_{i,j-1}}{2h} \\ \frac{\partial^2 \psi}{\partial x^2} &\approx \frac{\psi_{i-1,j} - 2\psi_{i,j} + \psi_{i+1,j}}{h^2} \\ \frac{\partial^2 \psi}{\partial y^2} &\approx \frac{\psi_{i,j-1} - 2\psi_{i,j} + \psi_{i,j+1}}{h^2} \end{aligned} \right\} \quad (15.9)$$

A similar approximate equation to eqn (15.9) is obtained for  $\zeta$ . Substitute these into eqns (15.7) and (15.8) and rearrange for  $\zeta_{ij}$  and  $\psi_{ij}$  respectively,

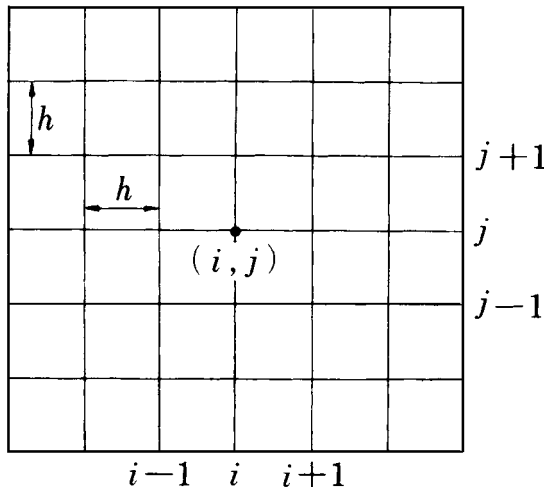


Fig. 15.3 Grid mesh and grid points

$$\zeta_{i,j} = \frac{1}{4}(\zeta_{i-1,j} + \zeta_{i,j-1} + \zeta_{i+1,j} + \zeta_{i,j+1}) + \frac{Re}{16}[(\psi_{i+1,j} - \psi_{i-1,j})(\zeta_{i,j+1} - \zeta_{i,j-1}) - (\psi_{i,j+1} - \psi_{i,j-1})(\zeta_{i+1,j} - \zeta_{i-1,j})] \quad (15.10)$$

$$\psi_{i,j} = \frac{1}{4}(\psi_{i-1,j} + \psi_{i,j-1} + \psi_{i+1,j} + \psi_{i,j+1} + h^2 \zeta_{i,j}) \quad (15.11)$$

Equations (15.10) and (15.11) show the relationship between vorticity  $\zeta_{ij}$  (as well as stream function  $\psi_{ij}$ ) at mesh points  $(i, j)$  in Fig. 15.3 and the vorticities (as well as stream functions) at the surrounding mesh points. If they are described for all mesh points, simultaneous equations are obtained. In general, because such equations have many unknowns and are also non-linear, they are mostly solved by iteration. In other words, substitute into eqns (15.10) and (15.11) the given values of the boundary condition on inlet section 1, the centre line and the wall face for  $\zeta$  and  $\psi$ . Set the initial value for the mesh points inside the area to zero. The values of  $\zeta$  and  $\psi$  will be new values other than zero when their equations are first evaluated. Repeat this procedure using these new values and the value obtained by extrapolating the unknown boundary value on outlet section 2 from the value at the upstream inner mesh point. When satisfactory convergent mesh point values are reached, the computation is finished. Figure 15.4 shows the streamlines and the equivorticity lines in the pipe obtained through this procedure when  $Re = 30$ .

This iteration method is called the Gauss-Seidel sequential iteration method. Usually, however, to obtain a stable solution in an economical number of iterations, the successive over-relaxation (SOR)<sup>1</sup> method is used.

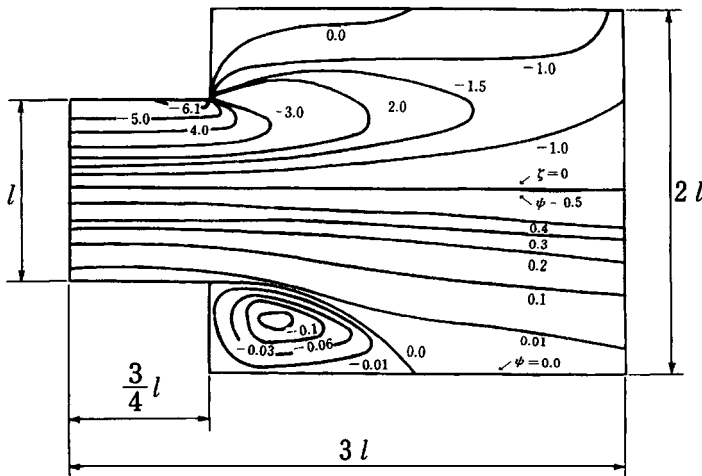


Fig. 15.4 Equipotentiality lines (upper half) and streamlines (lower half) of flow through sudden expansion

<sup>1</sup> Forsythe, G. E. and Wasow, W. R., *Finite-Difference Methods for Partial Differential Equations*, (1960), 144, John Wiley, New York.

Furthermore, when the left-hand side of eqn (15.7) is discretised using central differences, a stable convergent solution is hard to obtain for flow at high Reynolds number. In order to overcome this, the upwind difference method<sup>2</sup> is mostly used for this finite difference method.

This method is based upon the idea that most flow information comes from the upstream side. For example, if the central difference is applied to  $\partial\psi/\partial y$  of the first term of left side but the upwind difference to  $\partial\zeta/\partial x$ , then the following equations are obtained.

$$\frac{\partial\psi}{\partial y} = \frac{\psi_{i,j+1} - \psi_{i,j-1}}{2h} \quad (15.12)$$

and

$$\left. \begin{aligned} \frac{\partial\zeta}{\partial x} &= \frac{\zeta_{i,j} - \zeta_{i-1,j}}{h} && (\psi_{i,j+1} \geq \psi_{i,j-1}, \text{ when } u_i \geq 0) \\ &= \frac{\zeta_{i+1,j} - \zeta_{i,j}}{h} && (\psi_{i,j+1} < \psi_{i,j-1}, \text{ when } u_i < 0) \end{aligned} \right\} \quad (15.13)$$

Equation (15.13) is still only of first order accuracy and so numerical errors can accumulate, sometimes strongly enough to invalidate the solution.

### **Method using velocity and pressure**

In the preceding section, computation was done by replacing the flow velocity and pressure with the stream function and vorticity to decrease the number of dependent variables. In the case of complex flow or three-dimensional flow, however, it is difficult to establish a stream function on the boundary. In such a case, computation is done by treating the flow velocity and pressure in eqns (6.2) and (6.12) as dependent variables. Typical of such methods is the MAC (Marker And Cell) method,<sup>3</sup> which was developed as a numerical solution for a flow with a free surface, but was later improved to be applicable to a variety of flows. In the early development of the MAC method, markers (which are weightless particles indicating the existence of fluid) were placed in the mesh unit called a cell, as shown in Fig. 15.5, and such particles were followed. One of the examples is shown in Fig. 15.6, where a comparison was made between the photograph when a liquid drop fell onto a thin liquid layer and the computational result by the MAC method.<sup>4,5</sup>

More recently, however, a technique with the variables of flow velocity and pressure separately located (using a staggered mesh) as shown in Fig. 15.7 was adapted from the MAC method. Markers are not needed but are used only for the presentation of results.

<sup>2</sup> Gosman, A. D. *et al.*, *Heat and Mass Transfer in Recirculating Flow*, (1969), 55, Academic Press, New York.

<sup>3</sup> Harlow, F. H. and Welch, J. E., *The Physics of Fluids*, 8, (1965), 2182.

<sup>4</sup> Nakayama, Y. and Nakagome, H., (photograph only).

<sup>5</sup> Nichols, B. D., *Proc. 2nd Int. Conf. on Numerical Methods in Fluid Dynamics*, (1971), 371.

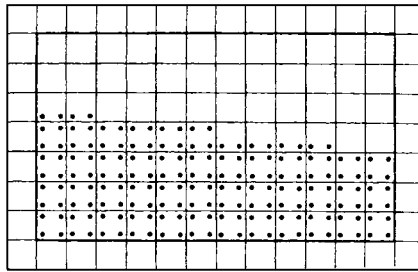


**Fig. 15.5** Layout of cell and marker particles used for computing flow on inclined free surface

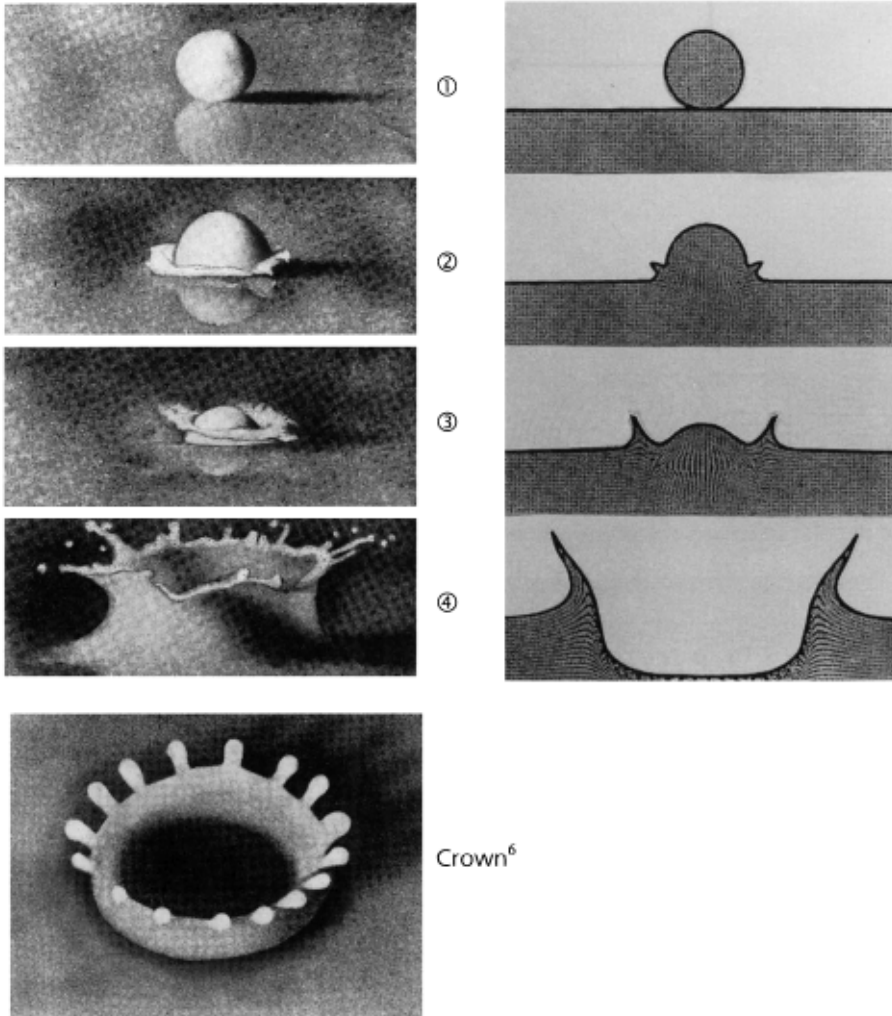


**Fig. 15.6** Liquid drop falling onto thin liquid layer: ① start; ② at 0.0002 s; ③ at 0.0005 s; ④ at 0.0025 s

<sup>6</sup> Fujii, K. and Nakagome, H., *Reading Physical Phenomena* (1978), 102, Kodansha, Tokyo (in Japanese).

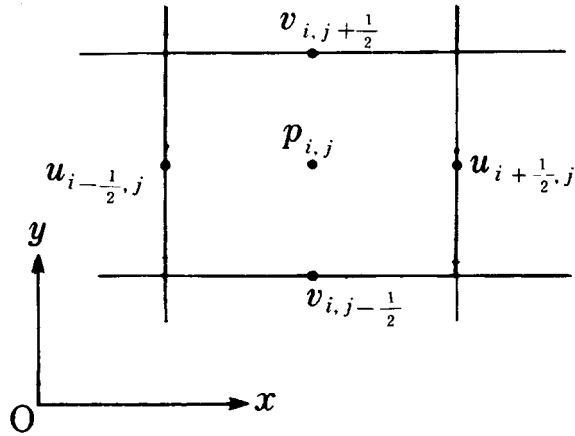


Fig. 15.7 Layout of variables in the MAC method

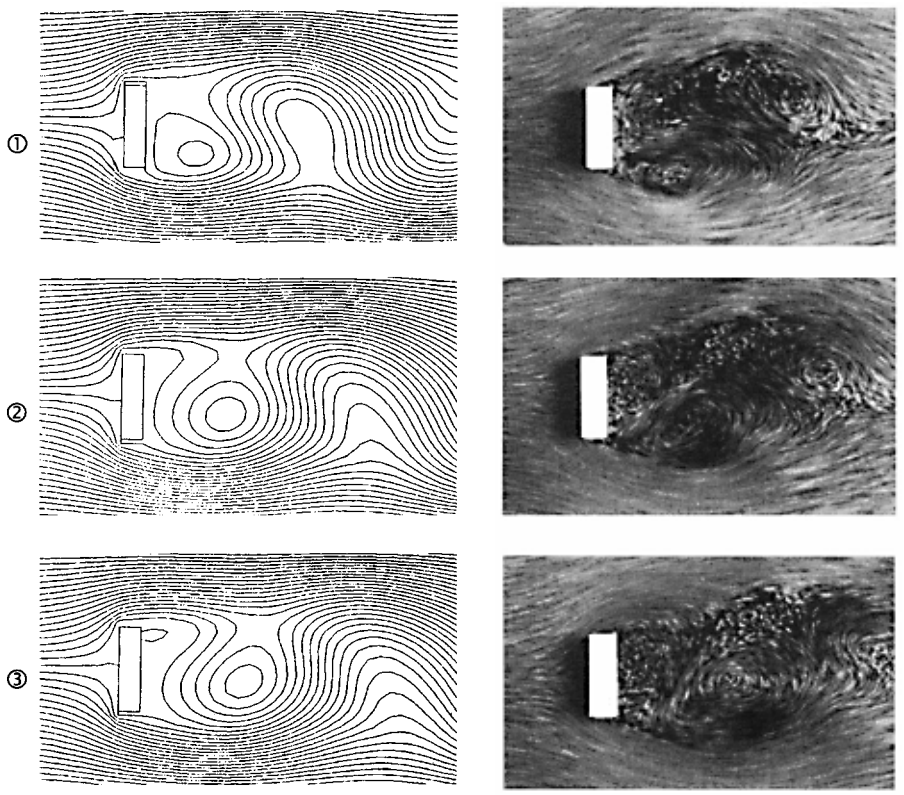


Fig. 15.8 Time-sequenced change of Kármán vortex street: ① start; ② at 0.1 s; ③ at 0.2 s

As an example, in Fig. 15.8 comparison is made between the kaleidoscopic change of Kármán vortices in the flow behind a prism and the computational result.<sup>7</sup>

### 15.1.3 Compressible fluid

#### *Time-marching method*

For a compressible fluid, the equation of a thermodynamic quantity in addition to the equations of continuity and momentum must be evaluated. One-dimensional isentropic flows etc. are solvable analytically. However, the development of a multi-dimensional shock wave, for example, can be solved by numerical methods only. For example, in the MacCormack method,<sup>8</sup> the differential equation is developed from the conservation form<sup>9</sup> for the mass, momentum and energy, neglecting the viscosity.

Figure 15.9 is the equi-Mach-number diagram of a rocket head flying at supersonic velocity calculated by using this method.<sup>10</sup>

One of the methods used to solve the compressible Navier–Stokes equation taking the viscosity into account is the IAF (Implicit Approximate

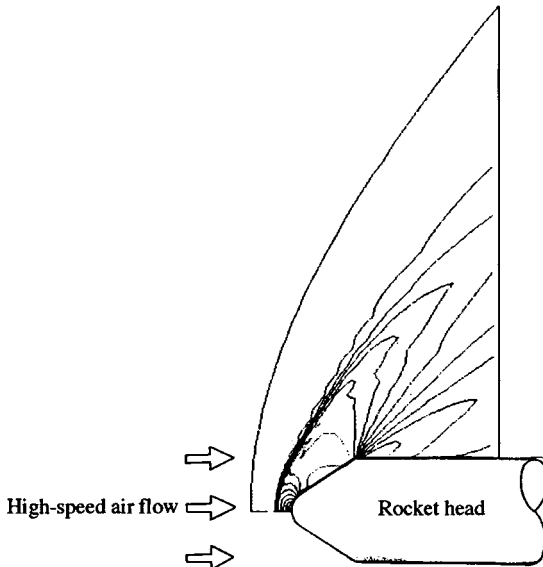


**Fig. 15.9** Equi-Mach number diagram of rocket nose in supersonic flow

<sup>7</sup> Nakayama, Y., Aoki, K. and Oki, M., *Proc. 3rd Asian Symp. on Visualization*, (1994), 453.

<sup>8</sup> MacCormack, R. W., *AIAA Paper*, 69-354, (1969).

<sup>9</sup> The conservation form of a one-dimensional inviscid compressible fluid is

$$\frac{\partial f}{\partial t} + \frac{\partial g}{\partial x} = 0 \quad f = \begin{Bmatrix} \rho \\ \rho u \\ e \end{Bmatrix} \quad g = \begin{Bmatrix} \rho u \\ p + \rho u^2 \\ u(e + p) \end{Bmatrix}$$

<sup>10</sup> Hirose, N. *et al.*, National Aerospace Lab., Japan.

Factorisation) method which is sometimes called the Beam–Warming method.<sup>11</sup> In Fig. 15.10 it is applied to a transonic turbine cascade. The solution is produced by using this method only for the region near the turbine cascade, while using the finite element method for the other region. Results matching the test result well are obtained.<sup>12</sup> As an example of a three-dimensional case, Plate 5<sup>13</sup> shows the result obtained by solving the compressible Navier–Stokes equation for the density distribution of the flow on the rotating fan blades and spinner of a supersonic turbofan engine by the IAF method.

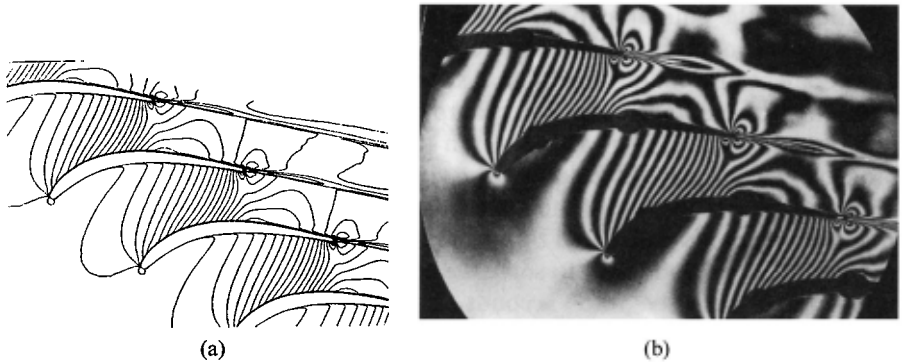


Fig. 15.10 Equidensity diagram of a transonic turbine cascade: (a) computation; (b) experiment (photograph of Mach–Zehnder interference fringe)

### Method of characteristics

Figure 15.11 is a test rig for water hammer, which is capable of measuring the pressure response waveform by the pressure transducer set just upstream of the switching valve. When the switching valve is suddenly closed, pressure  $p$  increases and propagates along the pipe as a pressure wave. To obtain its numerical solution, the wave phenomenon is expressed by a hyperbolic equation, and the so-called method of characteristics<sup>14</sup> is used.

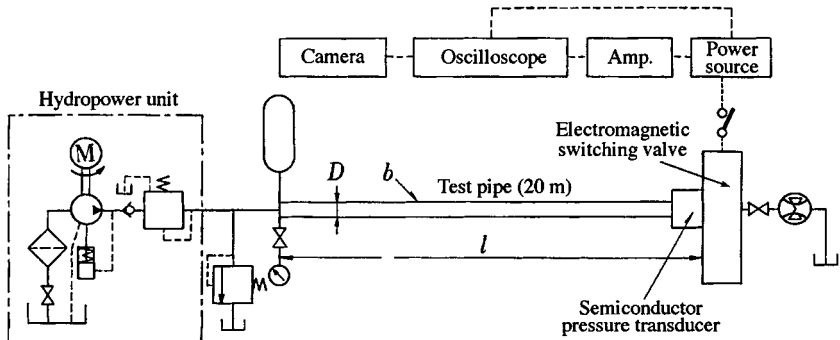


Fig. 15.11 Water hammer testing device

<sup>11</sup> Beam, R. M. and Warming, R. F., *AIAA Journal*, 16 (1978), 393.

<sup>12</sup> Nakahashi, K. *et al.*, *Transactions of the JSME*, 54, (1988), 506.

<sup>13</sup> Nozaki, O. *et al.*, *Proc. Int. Symp. on Air Breathing Engines*, (1993).

<sup>14</sup> Steerer, V. L., *Fluid Mechanics*, (1975), 6th edition, 654, McGraw-Hill, New York.

Now, putting  $f$  as the friction coefficient of the pipe and  $a$  as the propagation velocity of the pressure wave, linearly combine the continuity equation, which is the one-dimensionalised equations (6.1) and (6.12), with  $\lambda$  times the momentum equation, to get

$$\frac{\lambda}{\rho a^2} \left[ \frac{\partial p}{\partial t} + \left( v + \frac{a^2}{\lambda} \right) \frac{\partial p}{\partial x} \right] + \left[ \frac{\partial v}{\partial t} + (v + \lambda) \frac{\partial v}{\partial x} \right] + \frac{f}{2D} v |v| = 0 \quad (15.14)$$

Here, assume that

$$v + \frac{a^2}{\lambda} = \frac{dx}{dt} \quad v + \lambda = \frac{dx}{dt} \quad (\lambda = \pm a) \quad (15.15)$$

and partial differential equation (15.14) is converted to an ordinary differential equation. Furthermore, discretise it, and, as shown in Fig. 15.12,  $v$  and  $p$  of point P after time interval  $\Delta t$  are obtained as the intersection of the curves  $C^+$  ( $\lambda = a$ ) and  $C^-$  ( $\lambda = -a$ ) which are expressed by eqn (15.15) from the initial values of velocity  $v$  and pressure  $p$  at A and C.

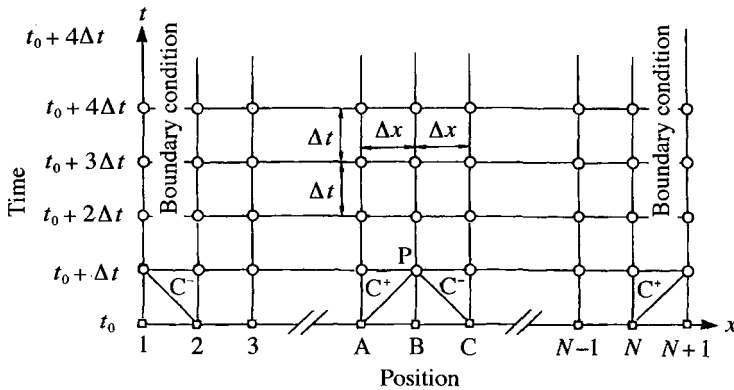


Fig. 15.12  $x$ - $t$  grid for solution of single pipe line

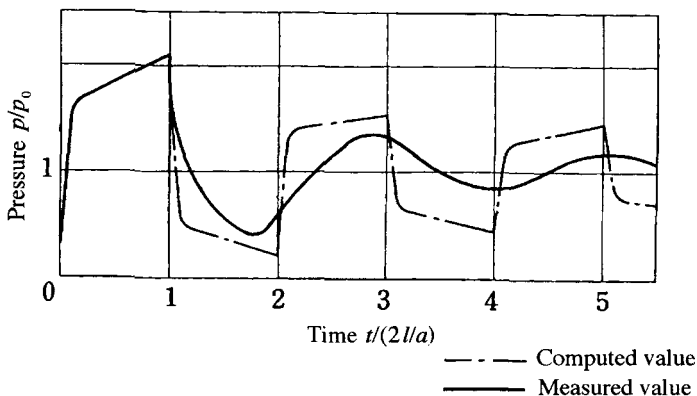


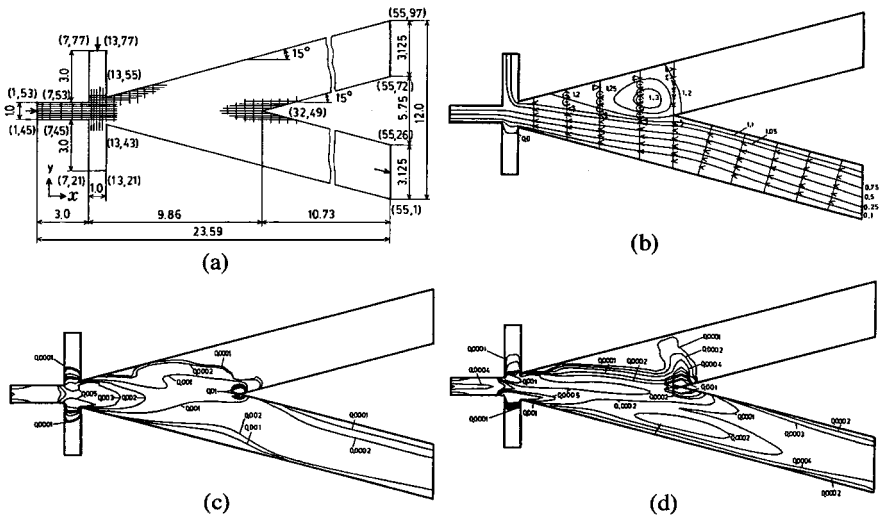
Fig. 15.13 Pressure response wave in water hammer action

Figure 15.13 shows the comparison between the pressure waves thus calculated and the actually measured values.<sup>15</sup> The difference between them arises from the fact that the frequency dependent pipe friction is not taken into account in eqn (15.14).

## 15.1.4 Turbulence

### *Turbulence model*

As already stated in Section 6.4, making some assumption or simplification for computing the Reynolds stress  $\tau_t$ , expressed by eqn (6.39), is called the modelling of turbulence. It is mainly classified by the number of transport equations for the turbulence quantity used for computation. The equation for which  $\tau_t$  is given by eqn (6.40) or (6.43) is called a zero-equation model. The equation for which the kinetic energy  $k$  of turbulence is determined from the transport equation, while the length scale  $l$  of turbulence is given by an algebraic expression, is called a one-equation model. And the method by which both  $k$  and  $l$  are determined from the transport equation is called a two-equation model. The  $k$ - $\epsilon$  model, using the turbulence energy dispersion  $\epsilon$  instead of  $l$ , is typical of the two-equation model. As an example, Fig. 15.14 shows the mesh diagram used to compute the flow in a fluidic device and also the computational results of streamline, turbulence energy and turbulence dispersion.<sup>16</sup>



**Fig. 15.14** Flow in a fluidic device: (a) mesh diagram; (b) streamline; (c) turbulent energy; (d) turbulent dispersion.  $Re = 10^4$ ,  $Q_c/Q_s = 0.2$  ( $Q_c$ : control flow rate;  $Q_s$ , supply flow rate)

<sup>15</sup> Izawa, K., MS thesis, Faculty of Engineering, Tokai University, (1976).

<sup>16</sup> Ogino, H. and Nakayama, Y., *Bulletin of the JSME*, 29 (1986), 1515.

### LES (Large Eddy Simulation)

In computations based on the time-averaged Navier–Stokes equation using turbulence models, time is averaged and the change in turbulence is treated as being smooth. However, a method by which computation can follow the change in irregularly changing turbulence for clarifying physical phenomena etc. is LES.

LES is a method where the computation is conducted by modelling only vortices small enough to stay inside the mesh in terms of local mean (mesh mean model), while large vortices are not modelled but computed as they are. Figure 15.15(a) shows a solution for the flow between parallel walls.<sup>17</sup> Comparing this with Fig. 15.15(b), a visualised photograph of bursts by the

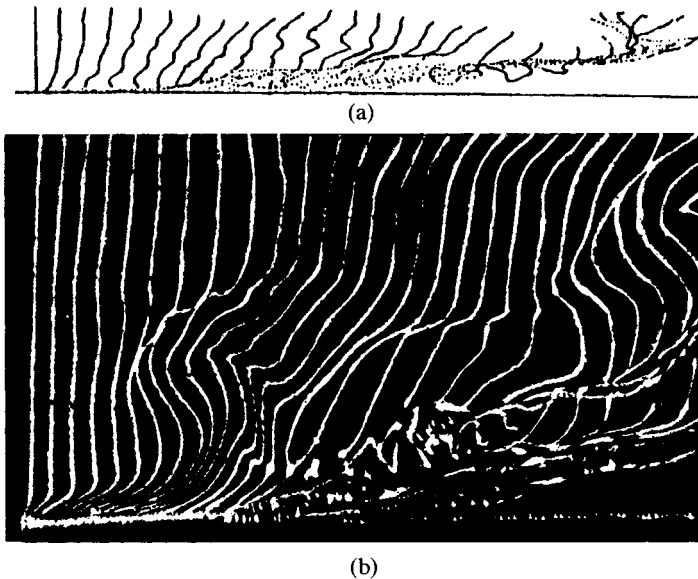


**Fig. 15.15** Time lines near the wall of a flow between parallel walls: (a) computed; (b) experimental

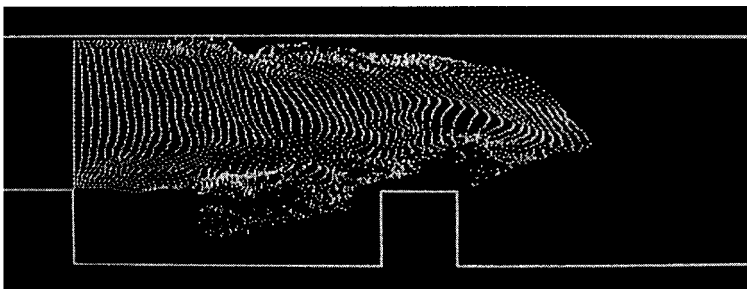


**Fig. 15.16** Turbulent flow over step (large eddy simulation). Reynolds number based on a channel width,  $Re = 1.1 \times 10^4$ .

<sup>17</sup> Moin, P. and Kim, J., *Journal of Fluid Mechanics*, 118, (1982), 341.

hydrogen bubble method,<sup>18</sup> it is clear that they coincide well with each other. In Fig. 15.16, the turbulent flow over a step is computed and its time lines are shown graphically.<sup>19</sup> Plate 2 shows the computational result for turbulent flow around a rectangular column.<sup>20</sup>

### Direct simulation

If the Navier–Stokes equation and continuity equation are computed directly as they are, then turbulence can be computed without using a model. This is called the direct simulation of turbulence. Even with the number of mesh points available in the latest large computer, only the larger turbulent vortices can be found. Nevertheless, interesting results on the large structure of turbulence have been obtained.<sup>21</sup>

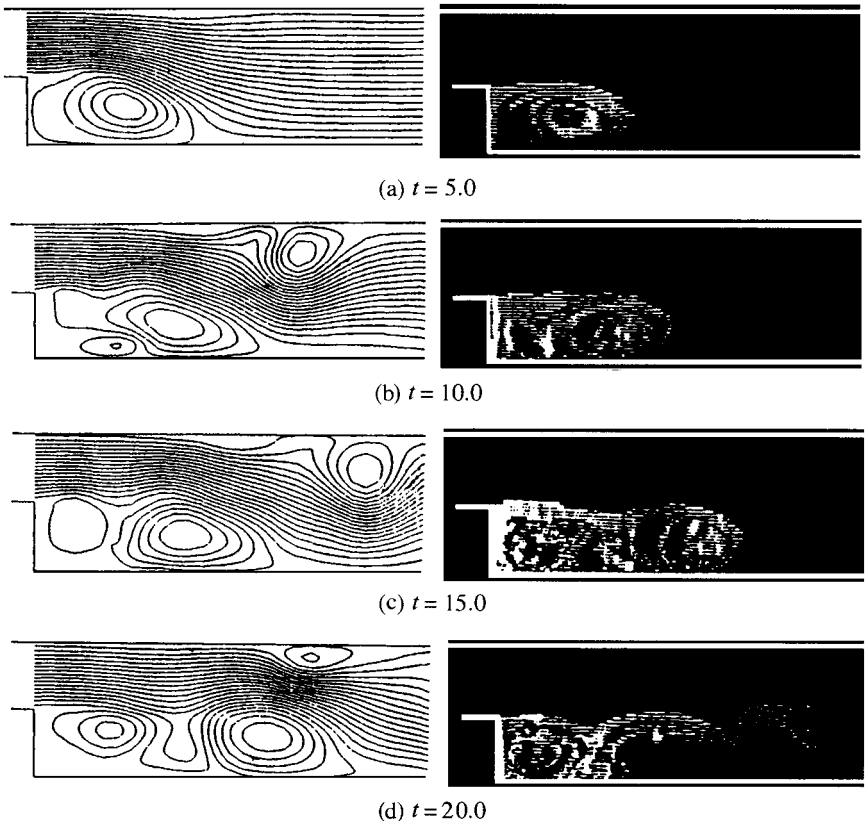


Fig. 15.17 Flow behind a step

<sup>18</sup> Kim, H. T. *et al.*, *Journal of Fluid Mechanics*, 50, (1971), 113.

<sup>19</sup> Kobayashi, T. *et al.*, Report IIS, University of Tokyo, 33 (1987), 25.

<sup>20</sup> Kobayashi, T., *Atlas of Visualization III*, Plate 10, (1997), CRC Press, Boca Raton, FL.

<sup>21</sup> Kuwahara, K., *Simulation of Turbulence*, *Journal of Japan Physics Academy*, 40, (1985), 877.

These methods simulate the movement of a large vortex by making the accuracy of the upwind difference scheme, shown in Fig. 15.13, of higher order and also by making the numerical viscosity<sup>22</sup> smaller. As one such example, the computed and visualised flows behind a step are shown in Fig. 15.17.<sup>23</sup> It can be seen that the movement of the vortex behind the step with the passage of time is well simulated.

## 15.2 Finite volume method

The finite volume method is a technique which discretises in a small region (the control volume shown in Fig. 15.18) the integration equation of the continuity equation and the Navier–Stokes equation written in conservative form.<sup>24</sup> The boundary volumes are then obtained using the neighbouring grid points.<sup>25</sup>

In the examples which appeared in the preceding sections, the grid was a regular structured grid in a line. Of late, however, the boundary-fitted grid following an irregular boundary or an unstructured grid has also been used. In the finite volume method, these new grids are easier to apply. As examples, the application of these techniques to an unstructured grid of triangles, the

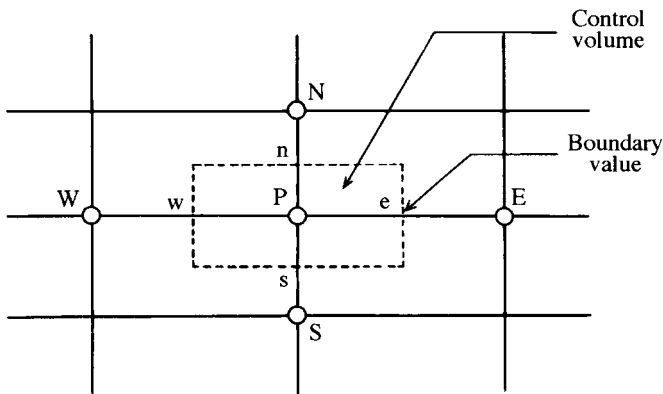


Fig. 15.18 Control volume

<sup>22</sup> This means the artificial propagation term produced by the finishing error of the upwind differential.

<sup>23</sup> Oki, M. *et al.*, *JSME International Journal*, 36-4, B (1993), 577.

<sup>24</sup> For example, the Navier–Stokes equation written in preservative form is obtained by expressing  $u\partial u/\partial x$ ,  $v\partial u/\partial y$ , etc., the inertia term of eqn (16.12), in the form of  $\partial(uu)/\partial x$ ,  $\partial(uv)/\partial y$ .

<sup>25</sup> Patankar, S. V., *Numerical Heat Transfer and Fluid Flow*, (1980), Hemisphere, New York.

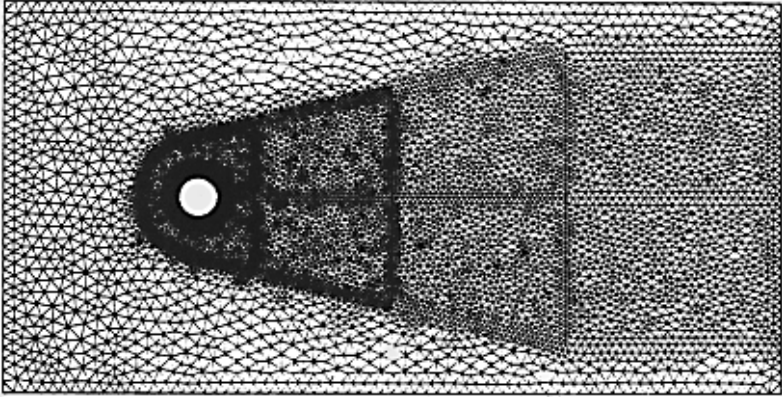


Fig. 15.19 Unstructured grid<sup>26</sup>

flow around a column, the mesh and the computed pressure distribution and velocity vector diagram are shown in Fig. 15.19 and Plate 1.

## 15.3 Finite element method

### 15.3.1 Division of elements

The finite difference method is a mathematical method by which the differential calculus appearing in the governing equation is directly approximated by finite difference equations. In the finite element method, however, by using physical approximations to discretise the differential equations, simultaneous algebraic equations are developed for the whole elements. Thus an approximate solution of the differential equations satisfying the boundary conditions is obtained. The flow zone was divided into a right-angled mesh as a rule in the finite difference method. In the finite element method, however, by dividing the area into proper-sized triangular or quadrangular elements as shown in Fig. 15.20, any complex-shaped area can be treated. The corners of the triangles or quadrangles are called nodal points, at which such variables as  $x$ ,  $y$ ,  $u$ ,  $v$  and  $p$  are defined.

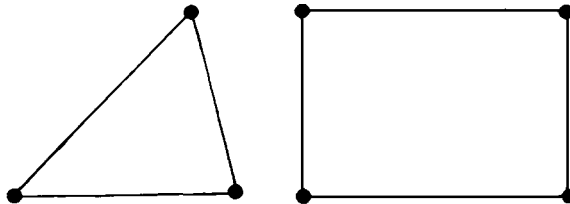


Fig. 15.20 Two-dimensional elements

<sup>26</sup> Oki, M. *et al.*, *Trans. JSME*, 65–631, B (1999), 870.

## 15.3.2 Method of weighted residuals

For discretisation by the finite element method, the variational principle or the method of weighted residuals is used. The variational principle is also called the minimum energy principle, which uses the principle that the potential energy is a minimum in the state of equilibrium. As this method has limited application, the method of weighted residuals is widely used.

Consider the potential flow around a cylinder placed between flat plates as shown in Fig. 15.21.

$$\left. \begin{array}{l} \text{in region S containing fluid} \\ \text{At inlet and on wall surface } S_1 \\ \text{At outlet } S_2 \text{ which is free boundary} \end{array} \right\} \begin{array}{l} \frac{\partial^2 \psi}{\partial x^2} + \frac{\partial^2 \psi}{\partial y^2} = 0 \\ \psi = \bar{\psi} \\ \frac{\partial \psi}{\partial n} = \frac{\partial \bar{\psi}}{\partial n} \end{array} \quad (15.16)$$

where the bars above the letters indicate that the applicable values are those on the boundary.

Next, in order to obtain the stream function  $\psi$ , multiply by a given function which is  $\psi^* = 0$  on boundary  $S_1$  (and can be any value in other areas by eqn (15.16)). Then integrate for the whole region. The following equation is obtained:

$$\int_S \left( \frac{\partial^2 \psi}{\partial x^2} + \frac{\partial^2 \psi}{\partial y^2} \right) \psi^* dA + \int_{S_2} \left( \frac{\partial \bar{\psi}}{\partial n} - \frac{\partial \psi}{\partial n} \right) \psi^* dS = 0 \quad (15.17)$$

Here, function  $\psi^*$  is called the weighting function. In eqn (15.17), assume function  $\psi^*$  and its derivative  $\partial \psi^* / \partial n$  are approximate values. The first term on the left expresses the quantity obtained by multiplying the error of the differential equation in the area (here, called the residual) by a given function and integrating for the whole area. Likewise, the second term expresses the quantity obtained by applying a similar process to the residual on boundary  $S_2$ . This is called a weighted residual expression. When the right solution is

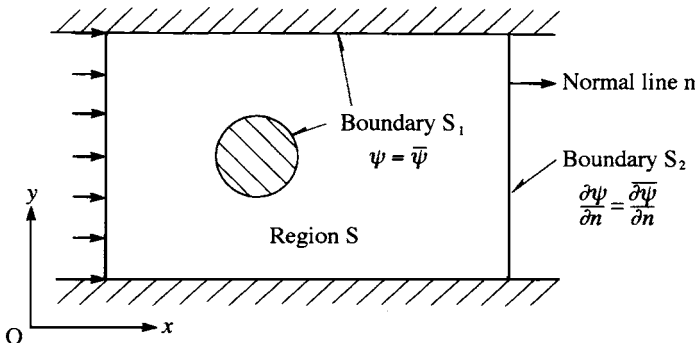


Fig. 15.21 Flow around cylinder

obtained, this equation applies strictly to the given function  $\psi^*$ . The approximate solution which distributes the error to satisfy the function  $\psi^* = 0$  is called the method of weighted residuals.

### 15.3.3 Interpolating function

In the finite element method, improvement is made by applying an algebraic equation derived using the values at nodal points to approximate the unknowns in each element. This equation is called an interpolating function. Where a weighting function of the same type is chosen it is called the Galerkin method.

It is not easy to obtain an approximate function effective all over sections  $[a, b]$  for the one-dimensional function  $\psi = \psi(x)$  shown in Fig. 15.22. Nevertheless, the section  $[a, b]$  can be divided into large and small linear elements. For example, divide the subsection where the function changes abruptly into (1, 2), and divide the subsection of the gentler change into (3, 4). Then for each of them  $\psi$  can be expressed by a one-dimensional (linear) function.

In the two-dimensional case, as shown in Fig. 15.23, by using triangular elements their size can be determined to the extent that the functions are expressible by a one-dimensional function of coordinates according to how abruptly or gently the functional change is expected. In other words,

$$\psi = \alpha_1 + \alpha_2 x + \alpha_3 y \quad (15.18)$$

Assume the function values at the corners of triangle 1, 2 and 3 to be  $\psi_1$ ,  $\psi_2$  and  $\psi_3$  respectively, then

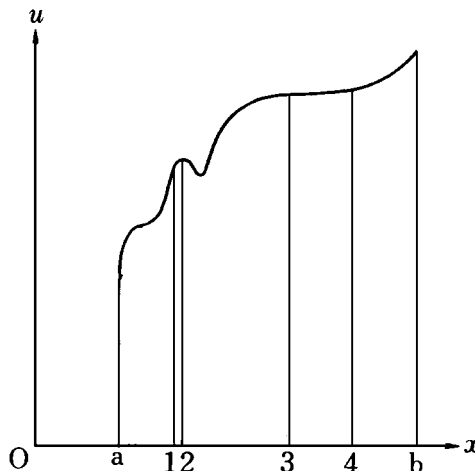


Fig. 15.22 One-dimensional function

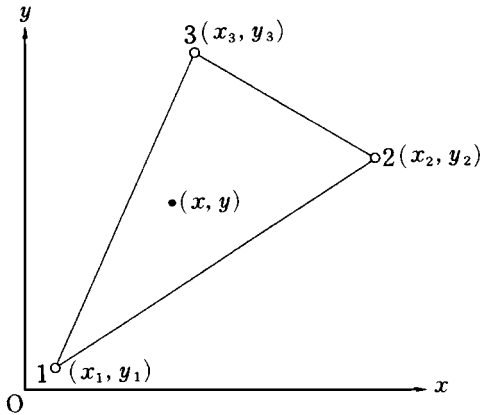


Fig. 15.23 Triangular element

$$\begin{Bmatrix} \psi_1 \\ \psi_2 \\ \psi_3 \end{Bmatrix} = \begin{bmatrix} 1 & x_1 & y_1 \\ 1 & x_2 & y_2 \\ 1 & x_3 & y_3 \end{bmatrix} \begin{Bmatrix} \alpha_1 \\ \alpha_2 \\ \alpha_3 \end{Bmatrix} \quad (15.19)$$

From the above,

$$\begin{Bmatrix} \alpha_1 \\ \alpha_2 \\ \alpha_3 \end{Bmatrix} = \begin{bmatrix} 1 & x_1 & y_1 \\ 1 & x_2 & y_2 \\ 1 & x_3 & y_3 \end{bmatrix} \begin{Bmatrix} \psi_1 \\ \psi_2 \\ \psi_3 \end{Bmatrix} \quad (15.20)$$

Substitute eqn (15.20) into (15.18),

$$\psi = \phi_1 \psi_1 + \phi_2 \psi_2 + \phi_3 \psi_3 = \sum_{i=1}^3 \phi_i \psi_i \quad (15.21)$$

In other words,  $\psi$  is the interpolating function expressed as the linear combination of nodal point values  $\psi_i$ . Hence, in the following form,

$$\phi_i = a_i + b_i x + c_i y \quad (i = 1, 2, 3) \quad (15.22)$$

it is called the shape function, and  $a_i$ ,  $b_i$  and  $c_i$  are determined by the coordinates of the nodal points.

### 15.3.4 Equation-overlapping elements

Approximate the unknown function  $\psi$  and weighting function  $\psi^*$  respectively in eqn (15.17) by interpolating the functional equation (15.21) using the nodal point values in the element and the same equation with  $\psi$  changed to  $\psi^*$ . Substituting these functions into the weighted residual equation, which is the deformed equation (15.17), gives the quantitative relation for each element. By overlapping them, a simulated linear equation covering the whole analytical area is developed. By solving these equations, it is possible to obtain the values at each nodal point and thus to draw the streamline of  $\psi = \text{constant}$ .

### 15.3.5 Applicable cases

To compute the flow shown in Fig. 15.21, as this is the symmetrical flow, the upper half only of the flow is divided into large and small triangular elements as shown in Fig. 15.24. For the finite element method, it is enough, unlike the finite difference method, just to divide the flow section finely around the cylinder where the velocity changes abruptly.

The computed streamline and velocity vector are shown in Fig. 15.25.<sup>27</sup>

With the finite element method also, as for the finite difference method, analysis of viscous and compressible fluids is possible. More recently, computation using a turbulence model has been carried out. As examples for a viscous fluid, the computational result for laminar flow around a pipe nest is shown in Fig. 15.26,<sup>28</sup> while that for the turbulence velocity distribution of the flow in a clean room using the  $k$ - $\epsilon$  model is shown in Plate 3.<sup>29</sup>

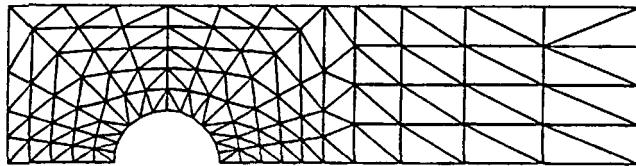


Fig. 15.24 Mesh diagram of flow around cylinder (180 elements and 115 nodes)

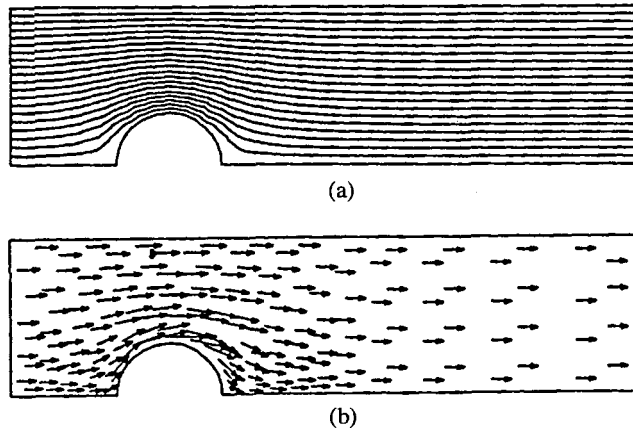
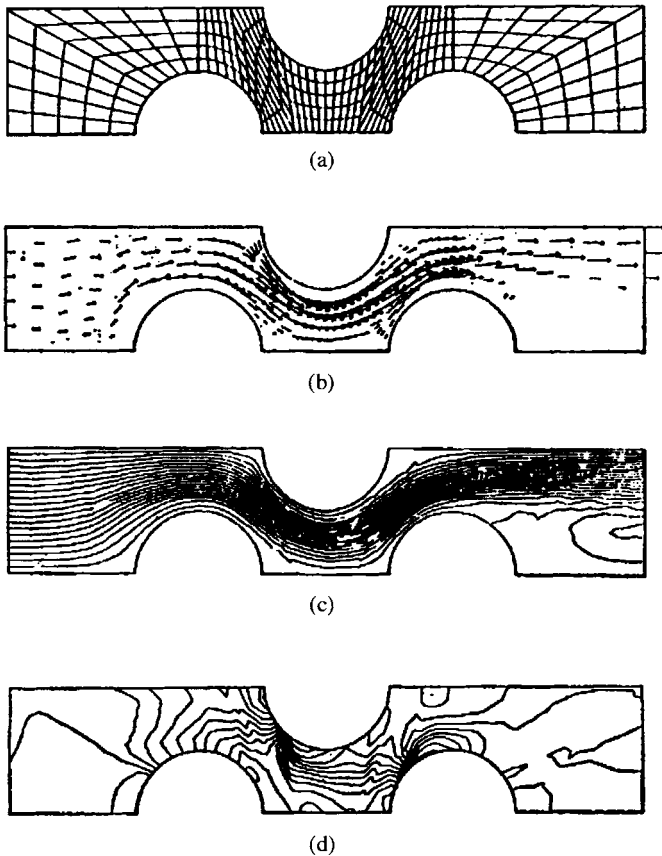


Fig. 15.25 Flow around cylinder: (a) streamline; (b) velocity vector

<sup>27</sup> Hayashi, K. *et al.*, *Flow Analysis by Personal Computer*, (1986), 73, Asakura-Shoten, Tokyo.

<sup>28</sup> Nakazawa, J., *Journal of JSME*, 87 (1984), 316.

<sup>29</sup> Ikegawa, M. *et al.*, *Proc. Int. Symp. on Supercomputers for Mechanical Engineering*, JSME, (1988), 57.



**Fig. 15.26** Flow around tube bank: (a) divided element; (b) velocity vector; (c) streamline; (d) pressure ( $Re = 100$ )

## 15.4 Boundary element method

Instead of solving the difference equation which governs fluid movement under the given boundary conditions, the boundary element method uses an integral equation which must satisfy values on the boundary. To derive the integral equation, one can use the method using Green's formula and also the method of weighted residuals. Green's formula method has long been used for analysing potential flow, and more recently has been systematised as the 'panel method', used for analysing external flows around aircraft, automobiles, etc.

Brebbia derived an equation by the more general method of weighted residuals with wider applicability, and named it the boundary element method.<sup>30</sup> It is often compared with the finite element method, and has been used in many fields of application.

<sup>30</sup> Brebbia, C. A., *The Boundary Element Method for Engineers*, (1978), Pentech Press, London.

In this method, the weighting function in the method of weighted residuals described in Section 15.3.2 is selected so as to satisfy the Laplace equation (15.16) within area  $S$ , and converted to an integral equation on boundary  $S_2$  surrounding the area as shown by the following equation:

$$\int_{S_2} \psi^* \frac{\partial \psi}{\partial n} dS - \int_{S_2} \psi \frac{\partial \psi^*}{\partial n} dS = 0 \quad (15.23)$$

Next, the boundary is divided into a number of line-segment elements. For example, in the case of the flow shown in Fig. 15.24, the mesh division is as shown in Fig. 15.27. Then, the value at a given point in the element is expressed in terms of the value of the nodal point by the interpolating equation (15.21) in the finite element method. The simultaneous linear equation for the value at the nodal points can then be solved.

The computational result for the case of Fig. 15.27 is shown in Fig. 15.28.<sup>30</sup> Here,  $\partial\psi/\partial n$  expresses the flow velocity along the boundary.

Since the boundary element method only requires division of the boundary of the region into the elements, it is popular for cases where the velocity or the pressure distribution on a body surface needs to be obtained.

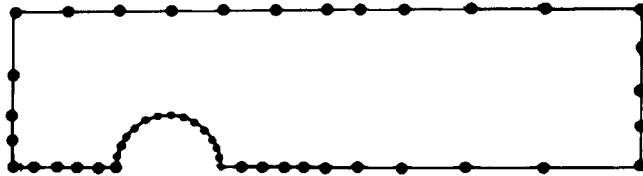


Fig. 15.27 Mesh diagram by boundary element method of flow around cylinder

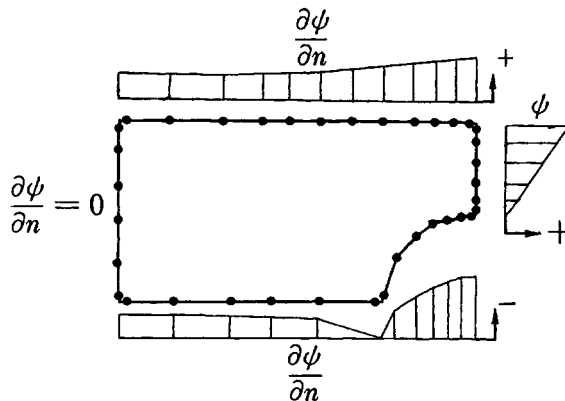
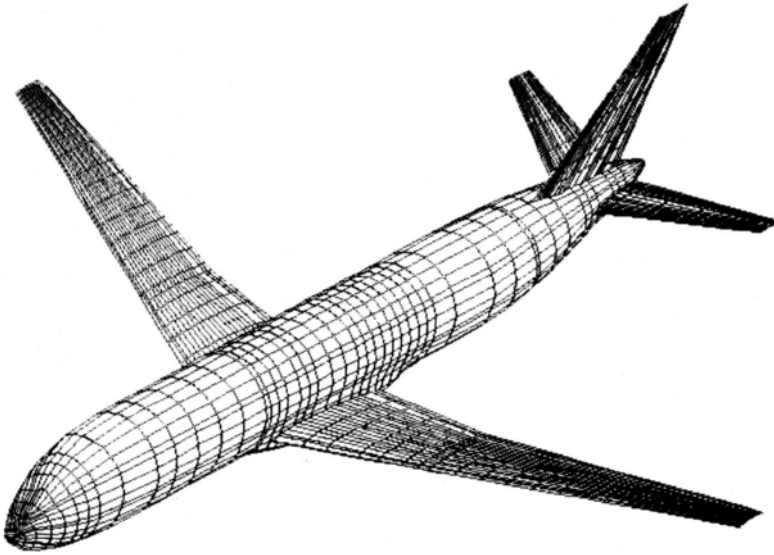


Fig. 15.28 Solution by boundary element method

<sup>30</sup> Brebbia, C. A., *The Boundary Element Method for Engineers*, (1978), Pentech Press, London.



**Fig. 15.29** Mesh diagram for computing flow around full model of transonic plane

Figure 15.29 is the mesh diagram for the case of flow around a full model of a transonic plane using the panel method. The computational result of the pressure distribution obtained is shown in Plate 6(a), which coincides very well with the result of the wind tunnel experiment as shown in Plate 6(b).<sup>31</sup>

Finally, a new kind of finite volume method has been proposed. This

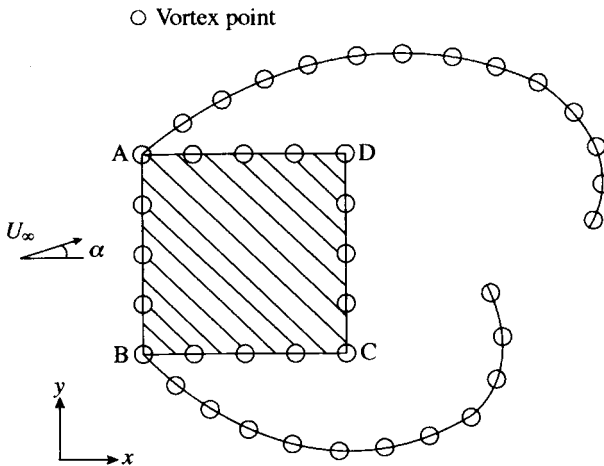


**Fig. 15.30** Modelling by discrete vortex element

<sup>31</sup> Kaiden, T. *et al.*, *Proc. 6th NAL Symp. on Aircraft Computational Aerodynamics*, (1988), 141.

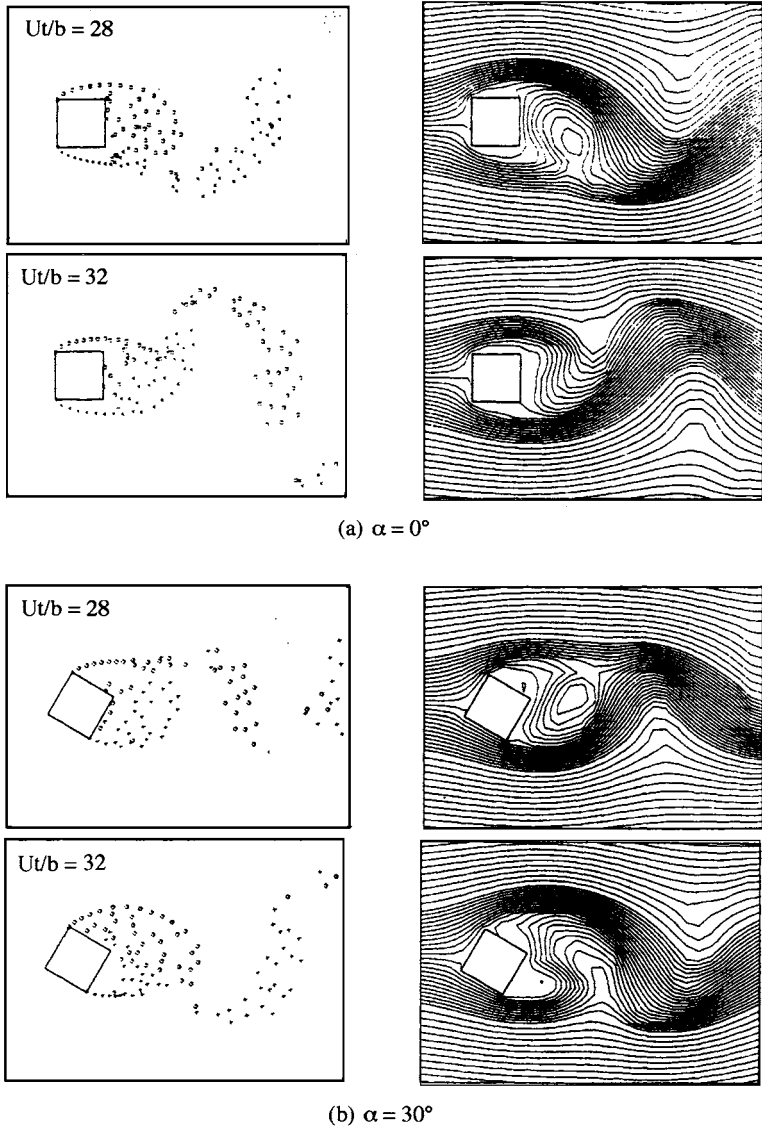


**Fig. 15.31** Flow pattern around the rectangular column illustrated in Fig. 15.30

technique replaces the successive distribution of vorticity produced in a flow field containing varied viscosity and density with discrete vortex elements. Each vortex motion is followed by the Lagrange method and thus analyses the unsteady flow field. This technique is called the discrete vortex method. As an example, the computational results for an unsteady flow around a square column in a uniform flow are shown in Fig. 15.30.<sup>32</sup>

<sup>32</sup> Inamoto, T. *et al.*, *Finite Element Flow Analysis*, University of Tokyo Press, (1982), 931.

In Fig. 15.31(a) and (b) the left and right sides show respectively the flow pattern of vortex points and streamlines. In any of these cases, the positive vortex (clockwise rotation) develops from point A and the negative vortex (counterclockwise rotation) from points B and C. These vortices develop behind the rectangular column and the Kármán vortex street is formulated in the wake.